CHAPTER THIRTEEN

Enzymatic control over coacervation

Karina K. Nakashima[†], Alain A.M. André[†], and Evan Spruijt*
Institute for Molecules and Materials, Radboud University, Nijmegen, The Netherlands
*Corresponding author: e-mail address: e.spruijt@science.ru.nl

Contents

Abstract

The discovery of membraneless organelles (MLOs) formed by liquid-liquid phase separation raised many questions about the spatial organization of biomolecular processes in cells, but also offered a new tool to mimic cellular media. Since disordered and charged protein domains are often necessary for phase separation, coacervates can be used as models both to understand MLO regulation and to develop dynamic cellular-like compartments. A versatile way to turn passive coacervate droplets into

[†] Equal contributions.

Methods in Enzymology, Volume 646
ISSN 0076-6879
https://doi.org/10.1016/bs.mie.2020.06.007

active and dynamic compartments is by introducing enzymatic reactions that affect parameters relevant for complex coacervation, such as the charge and length of the components. However, these reactions strictly take place in a heterogeneous medium, and the complexity thereof is hardly addressed, making it difficult to achieve true control. In this chapter we help close this gap by describing two coacervate systems in which enzymatic reactions endow coacervate droplets with a dynamic character. We further highlight the technical challenges posed by the two-phase systems and strategies to overcome them.

Abbreviations

α	monomer charge of polyelectrolytes A or B in Fig. 1(iii)
ϕ	volume fraction of polyelectrolytes A or B in Fig. 1(iii)
σ	charge density of polyelectrolytes A or B in Fig. 1(iii)
τ	turbidity
Abs	absorbance
ADP	adenosine diphosphate
ATP	adenosine triphosphate
$\mathbf{B_{eq\ dilute\ phase}}$	equilibrium concentration of coacervate component B in the dilute phase
$\mathbf{B_{eq\ dense\ phase}}$	equilibrium concentration of coacervate component B in the dense phase
Ddx3	DEAD box helicase protein 3
Ddx4	DEAD box helicase protein 4
DMF	dimethylformamide
DNA	deoxyribonucleic acid
EDTA	ethylenediaminetetraacetic acid
F	free energy of demixing for a two-component (A and B) solution in Fig. 1(iii)
FL	fluorescence
HK	hexokinase enzyme
HPLC	high performance liquid chromatography
I	light intensity
IDP	intrinsically disordered protein
k_B	Boltzmann constant
K	generic rate constant
$\mathbf{k_{cat}}$	apparent rate constant of enzymatic reaction
$\mathbf{K_M}$	substrate concentration for 1/2 maximal enzymatic reaction rate
K, $\mathbf{K_p}$	partitioning equilibrium constant
LLPS	liquid-liquid phase separation
LPP	lambda protein phosphatase
MEG-3	protein maternally expressed gene 3
MLO	membraneless organelle
N	number of monomers per polyelectrolyte chain in Fig. 1(iii)
NCK	cytoplasmic protein NCK1
NMR	nuclear magnetic resonance
N-WASP	neural Wiskott-Aldrich syndrome protein
PDMS	polydimethylsiloxane
PEG	poly(ethylene glycol)
PEP	phosphoenolpyruvate

PLE	poly-L-glutamic acid
PLL	poly-L-lysine
PNPase	polynucleotide phosphorylase enzyme
poly-U	polyuridylic acid
PSL	poly-L-serine-L-lysine
PVA	polyvinyl alcohol
PyK	pyruvate kinase enzyme
rDNA	ribosomal DNA
RGG	arginine-glycine-glycine domain
RNA	riboxy nucleic acid
rRNA	ribosomal RNA
$T_{\%}$	percentual transmittance
TAMRA	tetramethylrhodamine
TEV	tobacco etch virus
UDP	uridine diphosphate
UMP	uridine monophosphate
V_{in}	volume of the coacervate phase after centrifugation
V_{out}	volume of the dilute phase after centrifugation
V'	volume of the coacervate phase after dissolution with NaCl
V_{NaCl}	volume of salt solution required to dissolve the coacervate pellet

1. Introduction

Coacervates are dense liquid droplets of macromolecules, that were described in the early 20th century by Bungenberg de Jong and Kruyt (1929). In the case of complex coacervation, associative interactions between multiple soluble molecules, of which at least one is a macromolecule (*e.g.*, protein, DNA, RNA and other polymers), results in demixing into a polymer dense and a polymer diluted phase. The best studied complex coacervates are based on multivalent electrostatic interactions (but the phenomenon is not limited to those), and therefore responsive to environmental changes, such as pH, salt concentration and temperature (Brangwynne, Tompa, & Pappu, 2015; Spruijt et al., 2010). Coacervates have been widely used as analogs for liquid-liquid phase separated bodies identified in cells recently. Many membraneless organelles (MLOs), such as nucleoli, P-bodies and stress granules, have been proposed to form through liquid-liquid phase separation (LLPS) (Brangwynne et al., 2009; Shin & Brangwynne, 2017), controlled by enzymes. However, realizing a similar degree of dynamic control over coacervation as is common in cells is not a trivial task. In this chapter we

will present some tools to bring the expertise from physical chemistry to the study of coacervates as ideal *in vitro* models for MLOs and as dynamic compartments for cell mimicry.

In principle, any two oppositely charged macromolecules can undergo LLPS, but the area of the liquid phase in a phase diagram is affected by the strength of the interactions (Fig. 1). When interactions are too weak, the two-phase region is narrow and hard to find experimentally; when interactions are too strong, aggregation competes with LLPS at high concentration conditions. For complex coacervates, the strength depends, in addition to environmental factors, on two structural ones: the charge density and length of the poly-ions. Increasing charge density by adding small charged groups to the structure increases the electrostatic interaction energy

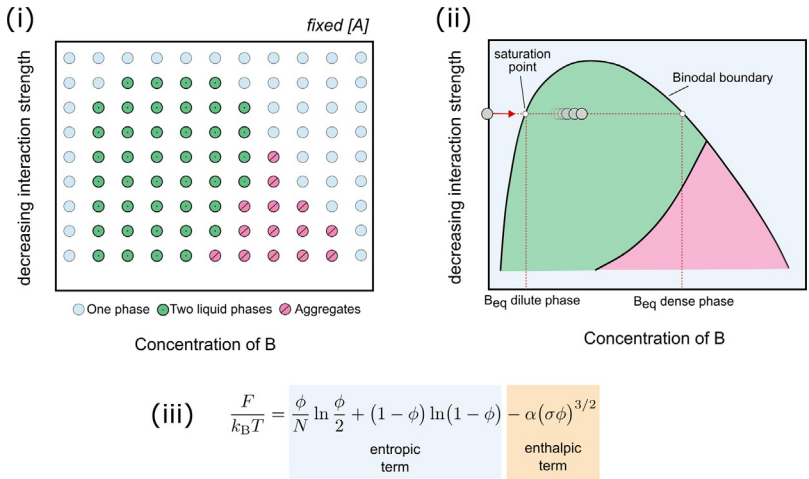

Fig. 1 Phase diagram for a two-component (A and B) complex coacervate. (i) Phase diagrams can be presented with a discontinuous plot, where each point represents a sample that was prepared and characterized by microscopy. (ii) An approximate continuous phase diagram can be built by interpolating the phase boundaries from the diagram in (i), or by determining critical points with a titration experiment (see Section 4). When the concentration of a polyelectrolyte A is fixed, increasing the concentration of B beyond the saturation point results in phase separation. The horizontal line in (ii) connects the two coexisting phases; the lowest concentration (of B) being the dilute phase. For some combinations of A and B aggregation can happen and depending on the structure, the pink area can expand further into the green two-phase region. (iii) The boundary between the phases can be estimated by minimizing the free energy of demixing *F*. For a more detailed account of the theoretical approaches to complex coacervation, please refer to Brangwynne et al. (2015), Spruijt et al. (2010) and Perry and Sing (2015).

(represented in a mean-field Voorn-Overbeek model by the term $\alpha\sigma^{3/2}$) (Brangwynne et al., 2015; Overbeek & Voorn, 1957). Increasing the length will decrease the relative importance of the mixing entropy and also favor the demixed state (Fig. 1(iii)). These structural dependencies introduce the possibility to control LLPS through reversible chemical modifications, similar to the way cells control condensates. For the purpose of biomimicry such modifications are much more relevant than environmental changes, such as variations in pH, that go beyond physiological conditions (Koga, Williams, Perriman, & Mann, 2011). The challenge to achieve control translates then into finding good reaction candidates to move along the horizontal line in Fig. 1(ii). Once achieved, such dynamically controlled coacervates can be used as a platform to investigate MLO regulation and function and as a tool for spatiotemporal organization in the context of a synthetic cell.

For use as *in vitro* models of MLOs, coacervates must capture the essential features of cellular condensates. MLOs are dense liquid droplets containing various intrinsically disordered proteins (IDP) usually together with nucleic acids (Banani, Lee, Hyman, & Rosen, 2017; Harmon, Holehouse, Rosen, & Pappu, 2017). LLPS is driven by associative interactions between low-complexity domains within the disordered regions of proteins (Banani et al., 2017; Elbaum-Garfinkle et al., 2015; Mitrea, Chandra, et al., 2018; Mitrea, Cika, et al., 2018; Nott, Craggs, & Baldwin, 2016), or between oligomerization domains or nucleic acid binding domains and RNA (Mitrea, Chandra, et al., 2018; Mitrea, Cika, et al., 2018; Mitrea et al., 2016). The underlying interactions are generally responsive to environmental conditions including pH, crowding, ionic strength and temperature. However, cells could never rely solely on (passive) environmental changes to control MLO formation, as these factors should be fairly constant in the cellular environment. Hence, control of multiple MLOs independently would not be possible.

Instead, MLO formation is commonly controlled by subtle chemical modifications on side groups of the IDPs or by binding to regulatory proteins (Nott et al., 2015; Qamar et al., 2018; Rai, Chen, Selbach, & Pelkmans, 2018). Both control mechanisms may be linked to the suggested role of MLOs in buffering of RNA (Maharana et al., 2018). An example is the spatial patterning of P-granules. Phosphorylation of MEG-3 by anteriorly enriched kinases promotes granule disassembly and leads to a posterior-rich gradient (Wang et al., 2014). MLOs can also function as bio-reactors, where the phase separation is used to control partitioning of

substrates and products (Case, Zhang, Ditlev, & Rosen, 2019; Li et al., 2012; Shin & Brangwynne, 2017). Reactions inside the MLO compartment could be enhanced as a result of higher concentrations (Case et al., 2019; Sokolova et al., 2013), but could also be limited when the substrate is not able to accumulate in the coacervate phase or when it interacts with the coacervate network (Banani et al., 2017; Shin & Brangwynne, 2017; Su et al., 2016). It is clear that enzymes play an important role in controlling intracellular phase separation, and they are therefore indispensable when studying coacervates as MLO models *in vitro*.

In the context of synthetic cells, dynamically controlled coacervates could serve as model systems for the complex, crowded intracellular milieu, helping solve traditional challenges in the field. Some benefits of coacervates over other synthetic cell compartments such as liposomes and polymersomes are: (i) coacervates reach a level of crowding closer to the cellular environment (Sokolova et al., 2013); (ii) transport of small molecules is not limited by a membrane, circumventing the need to incorporate, for instance, membrane proteins as pores (Mason, Buddingh, Williams, & van Hest, 2017); (iii) growth and division of coacervate droplets could be possible based on chemical reactions, if the underlying rates can be accurately matched to the coacervate phase characteristics (Te Brinke et al., 2018; Zwicker, Seyboldt, Weber, Hyman, & Jülicher, 2016). Some of these functions can rely on passive mechanisms, but to mimic cellular dynamics or life-like properties one has to look into active mechanisms, such as enzymatic control. But how do enzymes control coacervation in cells?

Enzymatic reactions can provide great control of coacervation because of their exceptional catalytic efficiency and well-defined conditions. It comes as no surprise that enzymes are heavily involved in the regulation of MLOs in cells. First of all, several examples have been reported where sidechains of proteins are modified by an enzyme, changing the charge density that is required for coacervation, which corresponds to modulating the first structural parameter. In the case of arginine methylation (*e.g.*, Ddx4 and FUS) or lysine acetylation (Ddx3), the modification leads to weakening of the electrostatic interactions, hence condensates dissolve (Nott et al., 2015; Qamar et al., 2018; Saito et al., 2019). In a related manner, enzymes can also be involved in regulating a specific recognition interaction. For instance, Li et al. reported that phosphorylation of tyrosine is required for phase separation within the N-WASP signaling pathway (Li et al., 2012): Nephrin contains three phosphorylation sites that can interact with

NCK; each NCK protein contains three binding domains that interact with N-WASP. Fully phosphorylated nephrin thus has effectively nine binding sites for interacting with N-WASP.

Secondly, it is likely that a reaction catalyzed by a transferase, ligase, or polymerase will favor phase separation, as the product in these cases has an increased length. This corresponds to the second structural parameter of length. With increasing length of a disordered protein or nucleic acid, the number of charged interaction sites increases and the relative importance of the mixing entropy decreases. An example can be found in the nucleolus, an extensively studied membraneless organelle both *in vitro* and *in vivo* (Berry, Weber, Vaidya, Haataja, & Brangwynne, 2015; Feric et al., 2016; Wei et al., 2017). It is the site of ribogenesis and consists of three type of condensates. The core is centered around the rDNA repeat on the chromosome. Transcription of rDNA results in the formation of long pre-rRNA molecules out of nucleotides. The pre-rRNA molecules are further processed in the second condensate region, called the dense fibrillar component. Finally, in the outer granular component, pre-ribosomal particles are assembled.

These examples of sophisticated enzymatic control over intracellular condensation suggest that control over less complicated coacervate systems should be possible. However, using enzymes to control coacervation adds extra complexity to the physical chemical characterization of systems at hand, as enzyme partitioning and differential reaction rates must be taken into account (Nakashima, Vibhute, & Spruijt, 2019). In the following paragraphs we first discuss the fundamentals of enzymatic reactions in two phases, followed by two types of enzymatic networks to control coacervation through the structural factors introduced above.

2. Enzymatic reactions in two phases

Finding a suitable enzymatic reaction to increase the length or charge density of a particular molecule can be a challenging task on itself, especially for proteins, but even if such a reaction has been found, it still does not warrant full control over the system. Once the enzyme has catalyzed formation of enough of the phase separating form of a (macro)molecule (this is sometimes referred to as "droplet material"), the system enters a two-phase regime; initially the amount of dense phase (coacervates) may be negligible, but if concentrations, and thus the degree of supersaturation, are high enough, the volume can be comparable to that of the dilute phase and it

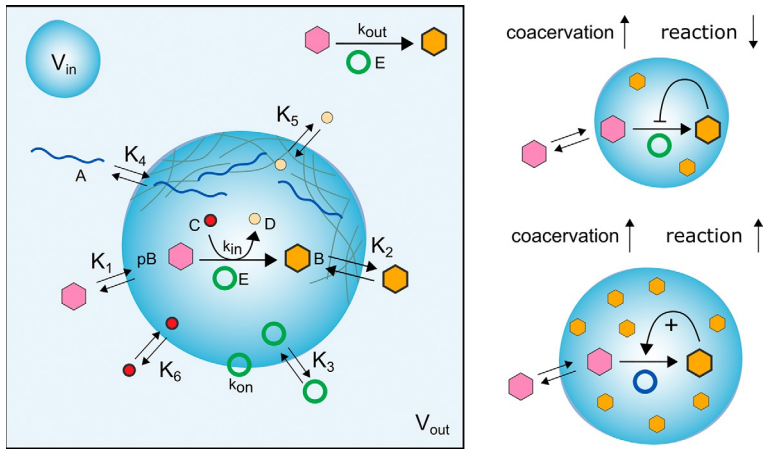

Fig. 2 Relevant factors for the reaction kinetics of a biomolecular reaction pB + C → B + D taking place in a two-phase system. An enzyme **E** converts a precursor **pB** into droplet material **B**, that complexes with **A** to form coacervates. Rate constants (k_{in}, k_{out}, k_{on}) might differ depending on the environment of the reaction and partitioning coefficients (K_i) affect the concentration and co-localization of all molecules involved. If the enzymatic reaction suffers from product inhibition, coacervation might limit its progression because of product accumulation; if product activation is possible, coacervation might lead to autocatalysis.

can be physically separated (Nott et al., 2015; Spruijt et al., 2010). The components of the enzymatic reaction, including the enzyme, substrate and possible cofactors, distribute over the two phases, and although there is free exchange between droplets and solution, the droplets represent a new chemical micro-environment. It is crucial to keep in mind the several added variables (Fig. 2): (i) additional rate constant in the droplet (k_{in}), (ii) new reactant and enzyme concentrations inside and outside of the droplets, (iii) partitioning coefficient of all components. These variables all affect the rate, location and outcome of the reaction. Moreover, it is relevant to control the rate at which the system enters the area under the binodal (Fig. 1) in order to avoid spinodal decomposition. If one of the purposes of enzyme-driven LLPS is to achieve spatiotemporal control over condensation, the parameters shown in Fig. 2 must be measured and known.

Specifics of enzymatic kinetics also come into play. Recent studies combining enzymes and LLPS rarely mention K_M and k_{cat} determination (exceptions are Davis et al., 2015; Yewdall et al., 2019), which could provide insight in how condensates affect biochemical reactions. Extreme differences in partitioning coefficients may result in a situation in which

Michaelis-Menten conditions no longer apply, making it difficult to modulate the kinetics to achieve the desired behavior (such as droplet growth, highly dependent on reaction rates (Zwicker et al., 2016)). Given how sensitive enzyme activity can be to the precise buffer conditions and other environmental factors, it may seem surprising that these reactions still proceed at all beyond the phase saturation point (Fig. 1(ii)), especially if the enzymes are taken up inside the droplets. For example, it has been taken for granted that pyruvate kinase (PyK) converts ADP to ATP in presence of poly-L-lysine to form coacervates (Nakashima, Baaij, & Spruijt, 2018), but it is not known how PyK overcomes the expected inhibition by ATP, which is now present at high concentrations inside the droplets.

We propose that enzyme-driven LLPS can benefit from a more detailed chemical characterization, and that approaching such systems as a two-phase reaction system is crucial for full control. This poses many analytical challenges as not all techniques are suitable for inhomogeneous mixtures. First, there is no straightforward method to quantify the extent of coacervation; one alternative is to measure the volume of the dense phase, but that cannot be done in a continuous manner. The most often used observable is turbidity (fraction of light scattered at a wavelength where the sample is transparent and non-absorbing, normally 500–700 nm) (Kaibara, Okazaki, Bohidar, & Dubin, 2000), which is an indirect measurement of the amount of droplets, and not a proof of the formation of liquid condensates. Still, for small timescales (minutes) it may correlate well to the progress of a reaction that results in the formation of droplet material. For longer observation periods, the gravitational settling of the droplets, coalescence or their adhesion to the walls of the well plate where the measurement is normally performed, start to interfere by decreasing turbidity even if the amount of droplet material remains the same. It is important to note this will also affect absorbance measurements performed in emulsions at any wavelength.

Turbidity measurements in a plate reader must be paired with microscopy to demonstrate the liquid nature of the condensates, as thin solid aggregates in suspension may be confused with an emulsion of liquid droplets based on turbidity alone. Microscopy is the most reliable technique to quantify components inside and outside the coacervate droplets, with the advantage of analyzing the two phases separately, while turbidity is a bulk measurement. The drawback is that covalent fluorescent labels are needed and their choice is crucial as to not drastically affect the structure (charge density or length) (Quinn et al., 2015) and the enzymatic activity. An additional requirement of microscopy is that, in order to monitor coacervates

as single droplets, with a stable position over time, the observation surface must be treated to minimize wetting. With regular and non-interacting surfaces (*e.g.*, PVA, PEG), the midplane of the droplets directly on the glass can be analyzed for extended periods, as a way to prove the condensation process and to estimate the volume of coacervate phase.

Typical reaction-monitoring techniques—chromatography, mass spectrometry, NMR—can be used for the emulsion as a whole, or for the phases separately. The former will always require a homogenizing step to prevent fluctuations in the signal across the sample or aggregation during injection. This makes it challenging to study fast kinetics of reactions in coacervates, but it may be the only available alternative for small molecule-based coacervates, when fluorescent labeling is the most disturbing. It is also possible and sometimes essential to separate the coacervate phase and the dilute phase by centrifugation. However, for small-scale experiments, with a limited amount of protein, it will generate a supernatant and a tiny coacervate pellet, which must be diluted or dissolved again before analysis. In theory, this approach yields more information about the parameters displayed in Fig. 2, but it introduces another challenge of knowing the initial volume of the pellet with precision.

3. Control over coacervation by chain length and charge density

In order to describe a strategy as general as possible, we will use two emblematic examples of enzymatically controlled coacervation, one of each category previously described. For elongation-driven coacervation, we chose the system based on poly-U-spermine complexation reported by Aumiller, Pir Cakmak, Davis, and Keating (2016) and Marianelli, Miller, and Keating (2018), and the reaction catalyzed by polynucleotide phosphorylase shown in the work of Spoelstra, van der Sluis, Dogterom, and Reese (2020). For charge density-driven coacervation, we will apply our methods to the poly-L-lysine (PLL)-ATP coacervates driven by pyruvate kinase reported earlier by our group (Nakashima et al., 2018). For an overview of alternative systems to which our methods can also apply, we start by discussing some recent work that can be classified as charge or length-based.

3.1 Length-based coacervation

Controlling the chain length of macromolecules is a powerful tool to control coacervation. Two routes have been reported in literature. First, coacervate

dissolution can be achieved through shortening the chain length through a protease. Semenov et al. have shown a system where a poly-L-lysine-L-serine (PSL) was cleaved by trypsin (Semenov et al., 2015). Trypsin is a proteolytic enzyme that catalyzes the hydrolysis at the C-prime end of lysine and arginine residues in proteins. PSL is a positively charged polypeptide that forms coacervate droplets with, for instance, poly-L-glutamic acid. Trypsin degraded the polymer into smaller fragments of different lengths, but all were too short to phase separate with poly-L-glutamic acid at the pH and salt concentration used. As a result, the coacervate droplets dissolved and turbidity disappeared. Another example in which a protease was employed, involved the cleavage of tandem and triplet RGG-domains by Tobacco etch virus (TEV) protease (Schuster et al., 2018). Schuster et al. used the RGG-domain of the P-granule protein LAF-1, which is able to form coacervates by itself under very mild conditions (Elbaum-Garfinkle et al., 2015; Schuster et al., 2018). By coupling two or three of these RGG-domains with a TEV-recognition motif in the linker, they could obtain stable coacervates *in vitro*, without addition of any negatively charged polymer, such as RNA. The TEV-protease cleaved the tandem/triplet repeat, yielding short RGG species and resulting in dissolution of the coacervates. This example shows that also cleavage of larger protein domains can be used to control coacervation.

Second, increasing the length of a biomolecule already prone to phase separation can widen the two-phase region in its phase diagram and enhance the degree of coacervation. Banerjee et al. formed coacervates based on a short arginine-rich peptide, $(RRXXX)_3$ where X could be any uncharged, polar residue, with either poly-U or RNA (Banerjee, Milin, Moosa, Onuchic, & Deniz, 2017). They used a T7 polymerase to synthesize the RNA from nucleotides *in situ* using a DNA template, which resulted in enhanced coacervation. However, when the RNA concentration exceeded a certain threshold, coacervates started to dissolve as a result of the shift in the charge ratio of RNA to cationic peptide. Similarly, poly-U can form coacervates in combination with spermine as shown by Aumiller et al. (2016) and Marianelli et al. (2018). These coacervates have inspired Spoelstra et al. and Deshpande et al. to use a polynucleotide phosphorylase (PNPase) for active coacervation (Deshpande et al., 2019; Spoelstra et al., 2020). PNPase consumes nucleotide diphosphates (NDPs) in a reaction where a nucleotide monophosphate (NMP) is added to the 3′-end of an oligomeric seed RNA, hereafter referred to as RNA primer (Fig. 3A) (Beljanski, 1996). At low concentrations the RNA primer (U_{20} was used by Spoelstra et al.)

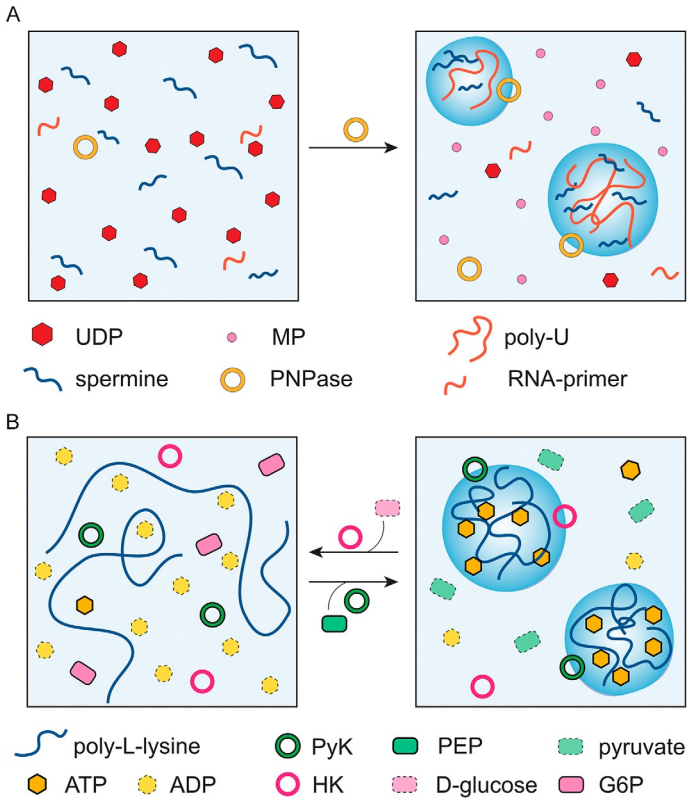

Fig. 3 Schematic representation of two model systems to control coacervation. (A) Length-based system. PNPase consumes UDP and incorporates UMP to a 20–24 nucleotides-long RNA primer, releasing a monophosphate (MP). The product is a long and polydisperse poly-U RNA-polymer which forms coacervates with spermine. (B) Charge-based system. PyK converts ADP and PEP to ATP and pyruvate, resulting in PLL-ATP coacervates. The reverse reaction, conversion of ATP and D-glucose to ADP and glucose-6-phosphate (G6P), is catalyzed by HK and dissolves the coacervates.

was unable to form coacervate droplets. As PNPase catalyzed the polymerization of NDPs, long RNA strands were formed and droplets emerged in solution as a result of nucleation and growth of spermine-RNA coacervates. Interestingly, PNPase was also able to catalyze the reverse reaction at high phosphate concentration, although the dissolution of coacervates took about three times longer than the assembly reaction (Spoelstra et al., 2020).

In Sections 4.2.1 and 4.3.1 we will focus on the latter example of length-controlled coacervation. We will discuss the parameters that should be taken into account when designing such a system, and we give a detailed protocol to realize dynamic control over coacervation in this system.

A few small adaptations were made compared to Spoelstra et al.: instead of using U_{20} as RNA primer, here we show this system can work for any type of oligo-RNA by using a $(ACUG)_6$ repeat as RNA primer.

3.2 Charge-density based coacervation

Changing length is not always a feasible route to control coacervation dynamics. Models based on subtle changes in charge-density might be better candidates to mimic the cellular control. We discuss two systems here that allow for both formation and dissolution of coacervates, controlled by enzymatic reactions.

One of the first reported examples of enzymatic control over coacervation came from Aumiller and Keating. They used a positively charged peptide repeat $[RRASL]_{2–3}$ to form complex coacervates with a long poly-U (Aumiller & Keating, 2015). Inspired by naturally occurring post-translational modifications, they used protein kinase A (PKA) to phosphorylate the serine residues in the peptide. The addition of effectively two negative charges per phosphate group decreased the net positive charge on the peptide, thereby weakening the interaction with poly-U and causing dissolution of the coacervates. They were able to reverse this process by dephosphorylating the peptide using lambda protein phosphatase (LPP). By controlling the addition of chemicals, such as EDTA which inhibits LPP, and ATP which is required by PKA for phosphorylation, this system shows great potential for out-of-equilibrium control.

A variation on this reversible phosphorylation system has been proposed by Nakashima et al. (Fig. 3B). In this scheme, coacervation is controlled by the concentrations of ADP and ATP, and their conversion is regulated by two enzymes (Nakashima et al., 2018). Pyruvate kinase (PyK) converts ADP to ATP by transfer of a phosphate group from phosphoenolpyruvate (PEP), thereby producing pyruvate. The ATP that is produced in this reaction formed coacervates with poly-L-lysine (PLL) that was present in solution. The reverse reaction, conversion of ATP back into ADP is linked to the phosphorylation of glucose to glucose-6-phosphate, catalyzed by hexokinase (HK). Without changing the initial ATP/ADP concentration, coacervation can be controlled by addition of the two co-substrates (PEP and glucose). This system was shown to be fully reversible and able to undergo repeated cycles of condensation and dissolution. In Sections 4.2.2, 4.3.2, 4.4 and 4.5 we will further explain how this system has been characterized.

4. Protocols

Here we present a detailed workflow to carry out the enzymatically controlled coacervate formation, protocols to observe and monitor the coacervate droplets, and protocols to quantify rates and partitioning (Fig. 4). We chose the two systems described above as examples, with a general strategy consisting of: determining the phase diagrams of the precursor and of the product (see Section 4.2); probing the enzymatic reaction in presence of the poly-ions with turbidity measurements (see Section 4.3); evaluating the control and kinetics of the reaction with microscopy measurements (see Section 4.4); and finally, characterizing the two phases separately (see Section 4.5). We start by describing the chemicals used and how they can affect the results; we then describe the protocols we used and highlight critical steps; and finally, in Section 5, we outline the steps to analyze the results.

4.1 Materials

Unless otherwise indicated all reagents were used as received from the manufacturer. All aqueous solutions were prepared in MilliQ water obtained from a MilliPore purification system, with an electrical resistivity of 18.2 MΩ cm at room temperature. Buffers were passed through a syringe filter (Nylon 0.22 μm) to prevent aggregation due to undissolved particles. Alexa labeling kits were ordered from Thermo Fisher, *N,N′*-bis(3-aminopropyl)-1,4-butanediamine (spermine) tetrachloride from TCI, and oligonucleotides Cy5-$[ACUG]_6$ and $[ACUG]_6$ from IDT. All other compounds mentioned below have been purchased from Sigma Aldrich.

Adenosine diphosphate disodium salt (ADP), adenosine triphosphate trisodium salt (ATP) and uracil diphosphate disodium salt (UDP) were separately dissolved in MilliQ water to prepare stock solutions of 0.50 M. Phosphoenolpyruvate potassium salt (PEP-K) was dissolved directly in 1.0 M HEPES buffer to make a 0.50 M PEP stock. The use of potassium salt avoided the need for other K^+ sources to activate pyruvate kinase. We found poly-L-lysine (PLL, HBr adduct) with the molecular weight in the range of 15–30 kDa to be ideal for our conditions, whereas chains of 52 kDa average (Alamanda Polymers) were more prone to aggregation with ATP, and chains of 4 kDa did not form condensates. A stock of 0.10 M PLL was prepared based on the molecular weight of the monomeric units, Lys-HBr (209 g mol^{-1}).

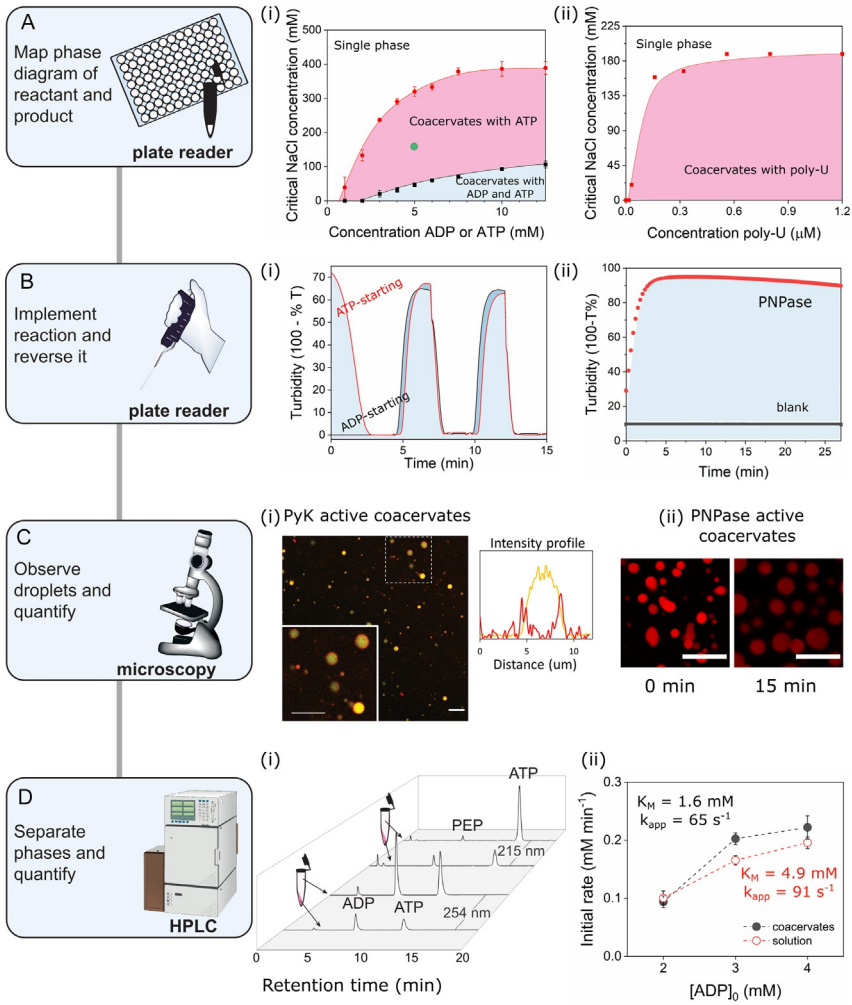

Fig. 4 General workflow to determine enzymatic control over coacervation and an overview of the results obtained. (A) Phase diagrams obtained from titration experiments for (i) PLL-ADP/ATP and (ii) spermine-poly-U mixtures. For further experiments (B–D) we chose the working salt concentration indicated by the green circle in A(i) for PLL-ADP/ATP, or no additional NaCl for spermine-poly-U. (B) Turbidity plots for reaction mixtures. B(i) shows the reversibility of phase separation upon addition of glucose (pink arrows) and PEP (green arrows) to the combined PyK/HK reaction mixtures. B(ii) depicts the increase in turbidity when the PNPase reaction is carried out. (C) Microscopic evidence of liquid condensates of (i) PLL-ATP and (ii) spermine-poly-U. In C(i), PLL was labeled with TAMRA and is shown in yellow, clearly coinciding with the droplets; PyK labeled with Alexa 647 is shown in red and can be seen in the interface of the droplets. The plot profile of a droplet in the insert highlights the

(Continued)

The concentrations we report are therefore of monomer, even when we refer to it as PLL. The stocks of 0.50 M concentration should be kept at −20 °C and used in the course of a month; the dilutions to 0.1 M kept at −20 °C were normally used within a week.

Polyuridylic acid potassium salt (poly-U, M_W 600–800 kDa, corresponding to about 2000–3200 bases), UDP, and RNA were dissolved in nuclease free water. Nuclease free water was prepared by autoclaving MilliQ water for 20 min at 121 °C. These stock solutions (see below for concentrations) were stored at −20 °C and used in the course of 3 months, with exception for the poly-U, which normally was used within a week.

Pyruvate kinase (PyK from rabbit muscle type VII, stocks prepared from a buffered aqueous glycerol solution) and hexokinase (HK from *Saccharomyces cerevisiae*, stocks prepared from lyophilized powder) stocks were kept at 4 °C, and dilutions in MilliQ water were prepared freshly in minimal volume, at the start of the experimental day. Polynucleotide phosphorylase (PNPase from *Synechocystis* sp.) stocks were kept at −80 °C, and during the day of the experiment diluted PNPase was stored at −20 °C.

4.2 Determining the coacervation window

Before implementing enzymatic control, we started by testing whether the conversion from reactant to product results in coacervation. We determined the phase diagram of the reactant and of the product under the same conditions, in order to find the region where the reactant does not form coacervates, but the product does—our "coacervation window" in Fig. 1. The experiment involves preparing the coacervates and determining the interaction strength at which they dissolve—we chose to do it by measuring turbidity during a salt titration, finding the critical salt concentration for each coacervate composition.

Fig. 4—Cont'd partitioning difference. For C(ii), poly-U labeled with Cy5 is seen in red also partitioned inside the droplets. (D) Chromatogram and reaction profiles obtained from quantitative analysis of the PLL-ATP mixtures. D(i) contains the chromatograms of the coacervate samples used to determine the partitioning of PEP and ADP. PEP and ADP have similar retention times, but the first is monitored at 215 nm, while ADP can also be detected at 254 nm. D(ii) is the result of the kinetic analysis of the PyK reaction mixture over time, after screening different initial concentrations of ADP and obtaining the initial velocity. *The diagrams in A(i) and B(i) were adapted from a previous paper in our group Nakashima, K. K., Baaij, J. F., & Spruijt, E. (2018). Reversible generation of coacervate droplets in an enzymatic network.* Soft Matter, 14*(3), 361–367. doi:10.1039/c7sm01897e.*

4.2.1 Coacervation window of oligo RNA and poly-U with spermine

Stock solutions	PNPase buffer (4×)	Passive poly-U-spermine coacervates
10% wt spermine tetrahydrochloride (494 mM) 1.0 wt% poly-U (<16 μM) 100 mM UDP 100 μM Cy5-$[ACUG]_6$ 1.2 M NaCl	400 mM Tris-HCl pH 9.0 4.0 mM EDTA 20 mM $MgCl_2$	1 × PNPase buffer 1.0 wt% spermine 0.0010 wt% up to 0.20 wt% poly-U

All in nuclease free water.

a. A dilution series of poly-U was prepared in a 96-well plate (flat, transparent bottom). Each well contained 60 μL of the reaction mixture. The poly-U concentration was varied from 0.0010 to 0.20 wt%, while the total volume was kept constant by adding MilliQ water. In wells containing more than 0.010 wt% poly-U, we observed a turbid mixture by eye and by plate reader (experiments described here were carried out at 30 °C on a Tecan Spark M10 multimode plate reader equipped with 0.5 and 1.0 mL injectors). To determine turbidity levels of individual wells, the absorbance was measured at 520 nm (bandwidth 3.5 nm, and a settle time of 50 ms).

b. A small volume (about 5 μL) was collected from each well and imaged with bright-field microscopy at a typical magnification of 40 × to confirm that no aggregates were present. The pH was checked with a paper strip.

c. The plate reader was subsequently prepared for the turbidity titration. The low-volume injector was first rinsed with MilliQ water and primed with the titrant solution, in this case 1.2 M NaCl.

d. The absorbance was followed at 520 nm (same settings as under **a**) in a repeated cycle of 2 μL injections (100 μL/s jet speed) of NaCl and linear shaking (1 mm amplitude, 1440 rpm frequency).

e. The injections were performed until the absorbance reached the value of a blank well (about 10 times).

f. This procedure was repeated by varying the concentrations of spermine to ultimately determine the optimal coacervate conditions.

Note: *when you do not have access to an automated injector, this procedure could also be performed manually with a micro pipette.*

4.2.2 Coacervation window of ADP and ATP with PLL

Stock solutions	Passive ADP/ATP-PLL coacervates
100 mM ADP	100 mM HEPES pH 7.4
100 mM ATP	5.0 mM PLL
100 mM PLL (15–30 kDa)	5.0 mM $MgCl_2$
0.50 M HEPES pH 7.4	1.0–10 mM ADP/ATP
100 mM $MgCl_2$	
0.50 and 1.0 M NaCl	

a. ADP-PLL mixtures (passive coacervates) were prepared with a fixed concentration of PLL, as described above, but with a varying concentration of ADP from 1.0 to 10 mM in steps of 1.0 mM. The samples were directly prepared in a 96-well plate (flat, transparent bottom). The volume was kept constant at 100 μL by adding MilliQ water. For most wells, some turbidity was visible upon gentle mixing with the pipette.

Note: *a high concentration of PLL was chosen for this screening to make sure that the nucleotides were limiting for coacervation; Mg^{2+} concentration was chosen to not limit PyK kinetics. The range of concentrations was chosen based on PyK common reaction conditions.*

b. A small volume, 5 μL, was collected from each well and imaged with bright-field microscopy at a typical magnification of 40 × to confirm that no aggregates were present. The pH was checked with a paper strip.

c. The plate reader (see details in Section 4.2.1**c**) was subsequently prepared for the turbidity titration. The low-volume injector of the plate reader was rinsed with MilliQ water and primed with the 0.50 M NaCl solution. Measurements were performed as described in Section 4.2.1**d** and **e**. For complete disappearance of turbidity, a maximum of 50 μL of titrant was needed (bringing the final volume up to 150 μL). The experiment was performed in triplicate.

d. For the phase diagram of ATP and PLL, the ADP stock was replaced with ATP. 1.0 M NaCl was used as titrant to minimize the total added volume. Importantly, all other concentrations and conditions were kept the same as in **a**. Steps **b** and **c** were repeated.

4.3 Conducting the enzymatic reactions to form and dissolve coacervates

After analyzing the data from the titrations and determining the phase diagram, we chose a "safe" NaCl concentration inside the coacervation window. For the UDP-spermine system we chose to add no salt; for the ADP-PLL, we used 130 mM NaCl. We then measured the turbidity of the reaction mixtures for enzyme-controlled coacervation over time, after the addition of the substrate or the enzyme.

4.3.1 PNPase reaction in presence of spermine

Stock solutions	PNPase buffer (4×)	PNPase reaction mixture
10% wt spermine (494 mM) 1.0 wt% poly-U (<16 μM) 100 mM UDP 100 μM Cy5-$[ACUG]_6$	400 mM Tris-HCl pH 9.0 4.0 mM EDTA 20 mM $MgCl_2$	1× PNPase buffer 5.0 μM oligo RNA (Cy5-$[ACUG]_6$ or $[ACUG]_6$) 15 mM UDP 1.0 wt% spermine 1 μM PNPase *(added just before measurement)*

a. A 30 μL PNPase reaction mixture was prepared without the enzyme and kept on ice. The PNPase enzyme was added just before the start of the turbidity measurement on the plate reader, and mixed gently by pipetting. Turbidity was measured every 10 s at 520 nm (bandwidth 3.5 nm) over a time course of 30 min.

b. The same preparation (**a**) was repeated for microscopy, adjusting the volume to 10 μL. We used an inverted confocal microscope (Leica TCS Sp8X), equipped with a HC PL APO 100 ×/1.40 (oil) CS2 objective and white light laser (20% power), 649 nm was used to excite Cy5-labeled RNA. Emission was recorded using a HyD detector in the range of 653–780 nm.

c. To study the influence of the PNPase enzyme, we varied the enzyme concentration between 0.50 and 2.0 μM, and the UDP concentration between 5.0 and 30 mM.

4.3.2 PyK and HK reactions in presence of PLL

Stock solutions	PyK reaction mixture	HK reaction mixture
100 mM ADP	100 mM HEPES pH 7.4	100 mM HEPES pH 7.4
100 mM ATP	5.0 mM PLL	5.0 mM PLL
100 mM PLL	5.0 mM $MgCl_2$	5.0 mM $MgCl_2$
(15–30 kDa)	5.0 mM ADP	5.0 mM ATP
0.50 M HEPES	130 mM NaCl	130 mM NaCl
pH 7.4	10 units mL^{-1} PyK	5.0 units mL^{-1} HK
100 mM $MgCl_2$	(approx. 80 nM)	(approx. 250 nM)
100 mM PEP	1% /v/v of Alexa-labeled PyK	5.0 mM D-glucose (*added just before measurement*)
100 mM D-glucose	(see Section 4.4.1)	
1.0 M NaCl	1% v/v of TAMRA-labeled PLL	
	(see Section 4.4.2)	
	5.0 mM PEP-K	

a. The reaction mixture of PyK was prepared directly in a 96-well plate. PEP was added just before the start of the turbidity measurement on the plate reader, and homogenized by gentle pipetting.

b. Turbidity was measured every 10 s at 520 or 550 nm depending on filter available for a time course of 30 min, with gentle shaking in between readings. The temperature was fixed to 30 °C.

c. The reaction mixture of HK was prepared in a 96-well plate. Glucose was added just before the start of the turbidity measurement on the plate reader and homogenized by gentle pipetting. Turbidity was measured under the same conditions as step **b**.

Note: *due to settling of coacervate droplets, when starting with ATP and PLL it is important to be fast to bring the system to a measurement, or the initial turbidity of different samples will vary too much.*

d. To perform cycles of coacervation-dissolution, PEP and glucose were added alternatively to the well, and the absorbance was measured at 550 nm. For manual addition, include a "plate out," "plate in" step in the measurement cycle. The substrate was added once turbidity has reached a maximum (glucose) or a minimum (PEP).

e. The addition of substrate experiment was repeated in a microscope chamber adjusting the total volume to 20–30 μL. We used a confocal microscope (Leica TCS Sp8), equipped with a HC PL APO 20 ×/0.75 (dry) CS2 objective and 552 and 638 solid state lasers (for rhodamine and Alexa 647 labeled components, respectively). Emission was recorded using a PMT detector at 570–700 and 650–700 nm.

4.4 Studying coacervate formation at a single droplet-level

From turbidity as a bulk measurement of coacervation, we move on to observing coacervate droplets individually by fluorescence microscopy. This involves fluorescent labeling of at least one of the polyelectrolytes and also of the enzymes, passivating the observation surface and preparing reaction chambers suitable for microscopy. From this microscopy-based study of coacervate formation, information about the droplets size and shape, and the partitioning coefficient of labeled components can be obtained.

4.4.1 Fluorescent labeling of enzymes

Labeling solutions
10 mg mL^{-1} Alexa-647 NHS ester in DMF (*ca.* 10 mM)
1.0 M $NaHCO_3$ pH 8.3
2 mg mL^{-1} PyK (50% aqueous glycerol solution, approx. 40 μM)

a. Enzymes were labeled using a Thermo Fisher Alexa-647-NHS-ester labeling kit and the accompanying instructions.

b. To a 500 μL of enzyme solution (around 2 mg mL^{-1} in a 50% glycerol solution), 50 μL of 1.0 M $NaHCO_3$ (pH 8.3) was added and mixed gently. Subsequently, 14 μL of the dye stock was added and incubated in a thermoshaker for 2 h at room temperature (20 °C).

c. Excess dye (unbound) was removed with a disposable centrifugal membrane filter unit (*e.g.*, VivaSpin concentrator). For PyK and HK, a molecular weight cut-off of 10 kDa was used (less than half the molecular weight of the enzyme). The membrane filter unit should be "blocked" first with a Tween-20 solution (0.1 wt%), to minimize irreversible adsorption of the enzyme or protein to the membrane, and rinsed five times with MilliQ water, and then with 10 mM phosphate buffer (pH 7).

d. After washing, the labeled protein was added to the centrifugal filtration tube and centrifuged at low speed (500 rpm) until it was concentrated to 250 μL. An equal volume of glycerol was added before storing at 4 °C.

Note: *the recommended storage conditions may vary depending on the type and stability of the enzyme. For example, the PNPase enzyme solution is stored at −80 °C as recommended by the manufacturer.*

4.4.2 Fluorescent labeling of poly-L-lysine

Labeling solutions
100 mM carboxytetramethylrhodamine (TAMRA) in DMF
100 mM 1-ethyl-3-(3-dimethylaminopropyl)carbodiimide (EDC) in DMF
100 mM N-hydroxysuccinimide (NHS) in DMF
200 mM PLL in MilliQ

a. PLL was labeled in a similar protocol as Section 4.4.1, using TAMRA as a labeling agent, together with EDC and NHS as activators. 50 μL of each stock described previously (TAMRA, EDC, NHS) were mixed and added to 430 μL of 0.20 M PLL solution in water. The reaction was left overnight in a thermoshaker at room temperature.

b. Excess dye was removed by concentrating the reaction mixture in a Centricon filter unit with a molecular weight cut-off of 5 kDa. Steps **c** and **d** in Section 4.4.1 were repeated for this sample, replacing the phosphate buffer with 10 mM HBr and eliminating the addition of glycerol.

4.4.3 Passivation of glass surfaces

General	PVA coating	PEGylation
Glass bottom petri dish (Cell-vis) Borosilicate cover glass (24 × 50 mm, thickness No. 1.5 from VWR) Ethanol 70% O_2-plasma or ozone cleaner	5.0 wt% Poly-vinyl alcohol (PVA, 87–89% hydrolyzed, 13–23 kDa from Sigma Aldrich) in MilliQ 5 min @RT	30 mg mL^{-1} mPEG-silane (M_n 5000 Da, from JenKem Technology) in toluene 1 h @65 °C

a. The stock solutions were prepared according to whether PVA or mPEG-silane were chosen. We observe that different coacervate compositions require different coatings for droplet stabilization.

b. The cover glass was cleaned with distilled water, 70% ethanol and MilliQ water, and then dried using pressurized air or nitrogen.

c. The glass surface was cleaned/activated using a plasma or ozone cleaner, according to the manufacturer's instructions for cleaning glassware. Plasma treatment will result in removal of any leftover contaminants on the glass surface, and expose surface hydroxyl groups that are required for modification.

d. The cover glass was incubated with either the mPEG-silane or the PVA solution, covering the surface with excess solution. We used 1 h at 65 °C (oven) for mPEG-silane, and 5–30 min at room temperature for PVA.

e. Subsequently, the glass surface was washed with copious amounts of MilliQ water and dried with compressed air or nitrogen. If the solution has dried during the reaction, the wash may require sonication. The glass surfaces were kept at 65 °C inside the oven until 1 h before use, or in a covered petri dish, and used in the course of 2 weeks.

4.4.4 Preparation of microscopy chambers

The required scale of the reaction was determined, depending on the total volume that must be added during the experiment. For example, an experiment in which coacervates are formed and dissolved alternatingly requires a larger volume than an experiment to determine the partitioning of a single enzyme. Here, we present two versions of microscopy chambers (Fig. 5).

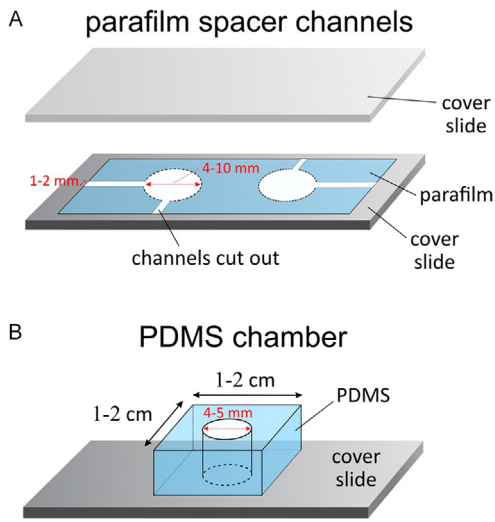

Fig. 5 Imaging chambers for fluorescent microscopy. (A) Parafilm-based chambers. (B) PDMS-based chambers.

We used the parafilm-sandwich layout for experiments in **a** and **b**, and PDMS chambers for experiments in **c** and **d**.

Parafilm chambers	PDMS chambers
PVA- or PEG-passivate coverslip (see Section 4.4.3)	Unmodified coverslip
Unmodified coverslip parafilm	Sylgard base and curing agent for silicone elastomer 184 kit (Dow Corning)

a. For up to 10 μL samples we made chambers from a parafilm-sandwich layout, as evaporation is minimized (Fig. 5). A rectangular piece of parafilm was taken (*ca.* 5 cm according to the coverslip length) and a small area was cut out with a puncher and a scalpel. We recommend the design shown in Fig. 5. The parafilm was then placed on top of the *passivated* face of the coverslip (observation surface), and covered with another coverslip.

b. To complete sealing, it was incubated for 10–15 min at 90 °C. Note: that longer incubation will improve the seal between the parafilm and the glass surfaces, but also lead to increased shrinking of the parafilm, which could cause trouble when adding your sample.

c. For up to 50 μL samples, we made the chambers from cured polydimethylsiloxane (PDMS). A mixture of Sylgard 184 base and curing agent in a 10:1 mass ratio was made, to obtain a moderately stiff silicone rubber. This mixture was placed in a petri dish Ø 35 mm inside a desiccator to remove air bubbles. Vacuum was applied for about 30 min. Holes of the desired volume were created by placing metal cylinders (Ø 4–5 mm, h 3–5 mm) into the silicone mixture (Fig. 5). The silicone mixture was baked at 65 °C for 90 min to obtain crosslinked PDMS that can be cut into smaller pieces.

d. The solidified PDMS was separated from the petri dish, and the cylinders were removed. The PDMS was then cleaned with detergent, MilliQ water, 70–100% ethanol, and finally dried in the oven at 65 °C.

e. The PDMS was cut in pieces smaller than the cover glass surface and stored on a piece of filter paper after covering the top and bottom sides with Scotch tape.

f. During the plasma or ozone cleaning of the glass surface (*before passivation*), the PDMS chambers were included, with the plain face (previously at the bottom of the petri dish) upwards. The glass and

the face of the PDMS that were exposed to plasma were bonded by pushing them gently together. For sealing, the glass with PDMS was incubated for 45 min at 90 °C.

g. The passivating agent (PVA or mPEG-silane) was added to the wells, and proceed as in Section 4.4.3**d** and **e**.

4.4.5 Determination of partitioning coefficients with fluorescence microscopy

Stock solutions	Passive ATP-PLL coacervates
100 mM ATP	100 mM HEPES pH 7.4
100 mM PLL (15–30 kDa)	5.0 mM PLL
0.50 M HEPES pH 7.4	5.0 mM $MgCl_2$
100 mM $MgCl_2$	5.0 mM ATP
1.0 M NaCl	130 mM NaCl
	1% v/v of Alexa-labeled PyK (see Section 4.4.1)
	1% v/v of TAMRA-labeled PLL (see Section 4.4.2)

a. ATP-PLL coacervates were prepared in volumes ranging from 0.10 to 1.0 mL.

b. Two variations of the passive coacervates were prepared: one with lower ATP concentration (*e.g.*, 3.0 mM) and one with higher PLL concentration (*e.g.*, 20 mM). This is to verify that K_p is independent of the concentration.

c. The samples were injected into the microscopy chambers as described above. The well was covered with a circular coverslip to minimize evaporation.

d. An image was recorded of a well filled with coacervate mixture but without fluorophore with the same laser settings to use as a blank. A blank was recorded for every filter cube or emission wavelength used.

4.5 Quantifying components inside and outside of the coacervate droplets

In this step we determine the concentrations of unlabeled components in the mixture using HPLC with UV/Vis detection. In general, this is required for small molecules or precursors, such as ADP, PEP and ATP in our examples. The determination of the partitioning coefficients in this case requires: (i) centrifugation of coacervate samples and separation of the

phases; (ii) estimation of the volume of each phase; (iii) dissolution and dilution to appropriate concentrations; (iv) HPLC analysis of the diluted samples. Additional quantitative data is obtained by following the PyK reaction over time, which involves quenching a sample from the reaction mixture at regular time intervals and preparing it for HPLC as outlined below.

4.5.1 Separation of the coacervate and dilute phase and volume estimation

Stock solutions	Passive ATP-PLL coacervates
100 mM ADP	100 mM HEPES pH 7.4
100 mM PEP	5.0 mM PLL
100 mM ATP	5.0 mM $MgCl_2$
100 mM PLL (15–30 kDa)	5.0 mM ATP
100 mM $MgCl_2$	130 mM NaCl
0.50 M HEPES pH 7.4	5.0 mM PEP or ADP
1.0 M NaCl	

a. 0.10–1.0 mL of ATP-PLL coacervates were prepared as described in Section 4.1. In order to measure the partitioning of PEP and ADP, those components were included, separately, in the ATP-PLL coacervate mixture the same concentration as in the reaction mixture (5.0 mM). Mix it by vortexing.

b. The sample was centrifuged at a low speed for an extended period. We used 3000 rpm and 30 min after observing that for shorter spinning times, the system had not reached a constant concentration (the determined concentration in the dilute phase were still slowly decreasing after 15 min due to very small coacervate droplets that had not settled yet). The low speed prevents the accumulation of a dense phase film (pellet) at the side wall of the eppendorf tube.

c. The dilute phase (supernatant) was collected carefully with a pipette by stopping just above the interface between the dense coacervate phase (bottom phase) and the dilute phase (top phase), to avoid contamination of the dilute phase with the coacervate phase. The collected dilute phase was transferred to a separate eppendorf tube. The amount was measured by setting the volume of the automatic pipette to an estimated value and attempting to aspirate all fluid with the pipette; the set volume

was adjusted until no liquid was left, and no air was aspirated. This was set as the volume of the dilute phase, $\mathbf{V_{out}}$. For the ATP-PLL system, $\mathbf{V_{out}}$ was very close to the total volume of the mixture.

d. The remaining dilute phase from the centrifuged tube was slowly collected using a thin pipette tip (0.20–10 μL). The volume of the pellet left behind (V_{in}) was measured by first dissolving it by adding a known volume of 1.0 M NaCl ($\mathbf{V_{NaCl}}$). This decreased the viscosity of the coacervate phase and facilitated easy handling by pipetting. Step **c** was repeated for the dissolved coacervate solution, obtaining V′. Calculate $\mathbf{V_{in}}$ as $\mathbf{V' - V_{NaCl}}$. For ATP-PLL coacervates prepared as stated, V_{in} is typically 1% of the total volume.

e. The typical concentrations determined in the ATP-PLL mixtures (5.0 mM in each component) are in the 0–10 mM range for the dilute phase, and 30–50 mM range for the dense phase. For that, we recommend for a first attempt, respectively, 100 × and 500 × dilution prior to HPLC injection.

4.5.2 HPLC analysis of the separate phases

Column	Eluents
Shim-pack WAX-1, 3 μm particles, 4.0 × 50 mm (anion exchange) 45 °C, 1 mL/min	20 mM phosphate buffer pH 7.0 **(A)** 480 mM phosphate buffer pH 7.0 **(B)**
Stock solutions	**Gradient program**
1.0 M KH_2PO_4 (500 mL) 1.0 M K_2HPO_4 (500 mL)	0–100% B in 20 min 100% B for 5 min 100–0% B in 5 min 0% B for 5 min

a. Each of the phases were diluted around 100 × before injection to reach concentrations around 100 μM (this may require several optimizations as concentrations are unknown *a priori*).

b. Detection at 215 and 254 nm (for PLL and PEP, and ADP and ATP, respectively) were used. The separation of the nucleotides required normal-phase HPLC with an anion exchange column in a gradient elution, as described in the chart above.

c. Using a calibration curve (peak area *vs* concentration), we determined the concentrations of the desired components considering dilutions (from $\mathbf{V_{out}}$ to the vial; from $\mathbf{V_{in}}$ to $\mathbf{V'}$ and then to the vial). If the final analyzed volume (with concentrations $A_{in,measured}$ and $A_{out,measured}$) was the same for both phases, the partitioning coefficient (K_p) of A was calculated as: $K_p = [A]_{in,measured} \times V_{out}/[A]_{out,measured} \times V_{in}$.

4.5.3 HPLC analysis of the reaction mixture over time

Stock solutions	PyK reaction mixture	PyK reaction mixture without PLL
100 mM ADP	100 mM HEPES pH 7.4	100 mM HEPES pH 7.4
100 mM PLL (15–30 kDa)	5.0 mM PLL	5.0 mM ADP
	5.0 mM ADP	130 mM NaCl
0.50 M HEPES pH 7.4	130 mM NaCl	10 units mL^{-1} PyK (approx. 80 nM)
100 mM $MgCl_2$	10 units mL^{-1} PyK (approx. 80 nM)	5.0 mM PEP
100 mM PEP	5.0 mM PEP	5.0 mM $MgCl_2$ (added at $t = 0$)
1.0 M NaCl	5.0 mM $MgCl_2$ (added at $t = 0$)	0.2% acetic acid (when quenching only)
10% v/v acetic acid	0.2% acetic acid (when quenching only)	

a. A 1.0 mL PyK reaction mixture was prepared as described in Section 4.1, including the PEP but leaving out the $MgCl_2$ (to make sure that the enzyme remains inactive until the start of the reaction). Adding the PEP before aliquoting minimized the effect of small variations among the samples on the final reaction rate.

b. The reaction mixture was split in 10 samples of 95 μL each and added to separate eppendorf tubes. 5 μL of the 100 mM $MgCl_2$ stock was added to each of the sample tubes, which were placed in a thermoshaker at 25 °C.

c. One tube at a time was quenched by adding 2 μL of 10% (v/v) acetic acid (the final pH should be around 3 and the turbid mixture should turn clear). The results from the turbidity measurement in protocol Section 4.3.2 were used to estimate the appropriate time intervals, keeping in mind the initial time points are crucial for K_M and k_{cat} determination.

d. The samples were diluted around 100× and we applied steps **b** and **c** in Section 4.5.2 to obtain the kinetic profile of ATP concentration.
e. The same procedure was used with a sample without PLL, as a "solution phase control."
f. Substrate concentrations were varied to obtain a typical Michaelis-Menten plot for coacervates and solution phase. For the PyK reaction, ADP could be varied from 2 to 5 mM while still working in the coacervation window.

5. Analysis

The protocols we proposed above provide all the data required to obtain the principal properties of a dynamic two-phase system: phase diagram, partitioning coefficients and reaction profiles. We now discuss how these properties can be determined from the raw turbidity data, microscopy images and chromatograms.

5.1 Phase diagrams from turbidity data

A first step to define the conditions under which a candidate enzyme could induce coacervation or dissolution is to plot the phase diagram(s). Although turbidity is not a direct and decisive measure of coacervation, it allows to determine the approximate dilute branch of the binodal in a fast and simple way. The disadvantage of the titration method is that the starting components (*e.g.*, polyelectrolytes) get diluted, so it is important to maximize titrant concentration and minimize additions. To confirm that turbidity is caused by the nucleation of liquid droplets, it is important to use microscopy, as aggregates in solution will also result in increased turbidity—though over time, turbidity will have much more noise for suspensions than for emulsions.

Turbidity is the level of transparency of a mixture, or the fraction of light that is not transmitted, but scattered. Turbidity (τ) is commonly defined for a sample without absorption as:

$$\tau = -\ln\left(\frac{I}{I_0}\right) \tag{1}$$

It can be calculated from the measured extinction ($\mathrm{Abs} = -\log_{10}(I/I_0)$), provided that no absorption of light occurs at the detection wavelength. It should therefore be measured at a wavelength far from absorption bands,

which is why we chose 520 or 600 nm. From the absorbance value, turbidity can be calculated using the following equation:

$$\tau = 2.3 \times \mathrm{Abs} \tag{2}$$

Information about the turbidity of samples is often reported as a derivative of transmittance ($T_{\%}$), or the percentage of light that is transmitted:

$$T_{\%} = 100\% \times \left(\frac{I}{I_0}\right) = 100\% \times 10^{-\mathrm{Abs}} \tag{3}$$

The transmittance ranges from 0% to 100%, and a plot of $(100 - T_{\%})$ indicates the amount of scattered light, and is sometimes also called turbidity. To determine the critical salt concentration, a plot of $(100 - T_{\%})$ as a function of the added salt concentration (NaCl) is made. Note that we did not take into account the total ionic strength of the solution, which would include counterions from ADP, ATP and PLL, but just the salt added. Dilution during titration was taken into account. At the critical concentration (C_s), the turbidity reaches zero (after baseline correction). If the turbidity did not reach zero, C_s can also be found from a linear fit of the points in the steepest part of the turbidity profile, and taking the x-intercept. We used this approach for our determination of the phase diagrams of both ADP-PLL and ATP-PLL. Usually the steepest decrease was found about 3–5 points before turbidity stabilized at its minimal value close to zero.

To obtain the phase diagram in Fig. 4A, C_s is plotted as a function of polyelectrolyte concentration—poly-U or ADP or ATP. It is important to notice the difference between the length- and the charge-controlled systems. In the case of spermine-poly-U, the substrate mixture contains no polymeric species (UDP, an RNA primer and spermine), and no stable coacervates can be formed under the PNPase reaction conditions. The product of the PNPase reaction, poly-U, does form coacervates with spermine, and C_s can be determined. However, since the exact length of the final product is unknown, the phase diagram can only be determined for a poly-U of a known molecular weight, and it should be used as an estimate of the PNPase product. These provisions apply to many elongation reactions, which can result in products with a distribution of lengths instead of a single composition (Banerjee et al., 2017). Transcription of a genetic construct is a notable exception to this. In the ATP/ADP-PLL case, a clear window between the two-phase region of each phase diagram is found.

Some modifications of our method are possible. First, we fixed the concentration one of the two interacting species (spermine and PLL, respectively), so that the phase diagram is technically obtained for different charge ratios (f_+, f_-). One could also fix poly-U, ADP or ATP concentration in order to find the optimal spermine or PLL concentrations (respectively), assuring that the system is always limited by the dynamic component. Second, we performed a salt titration (in which the titrant has a high ionic strength) to determine the critical salt concentration, but an alternative water titration (in which the titrant is MilliQ water or a low-salt buffer) of a sample prepared above the critical salt concentration normally gives the same value, highlighting the reversibility of LLPS. Finally, instead of C_s as the interaction parameter, temperature and pH could also be used.

Several factors will affect the coacervation window: (i) components in the enzyme stock may affect the interaction strength, (ii) substrates, products, and cofactors can also contribute to the overall ionic strength and narrow the window, and (iii) temperature strongly affects the diagram. It is important to realize that all components of a candidate reaction might have an influence on the process; ions in the buffers and secondary reaction products (such as pyruvate in the PyK reaction) have shown strong effects in solubilizing coacervates. As shown in Fig. 4A(ii), the phase diagram of poly-U with spermine is obtained at the exact conditions of the PNPase reaction, which requires alkaline conditions (pH 9). In our case, spermine is a stable positively charged molecule in a wide pH range, but deprotonation reduces the net charge and likely narrows the two-phase region.

Based on the phase diagrams, a working salt concentration and polyelectrolyte concentration were selected. The marked point in Fig. 4A indicates where coacervation is possible for a nearly 100% efficient reaction, and with some margin for the effect of secondary products (pyruvate, orthophosphate) and undetermined products (wide range of poly-Umers).

5.2 Reaction monitoring with turbidity

In Fig. 4B we show that plate reader experiments can be used to easily verify the reproducibility of the forward and reverse reaction of the PyK and HK controlled reactions. The green and orange arrows indicate substrate addition. For some of the enzymes the reaction is found to proceed very quickly, such as the PNPase reaction in Fig. 4B(ii). However, these

measurements only show the turbidity over time, or the turbidity in the presence of salt. To visualize that the mixture really contains coacervates, we have to go to microscopy experiments.

5.3 Partitioning coefficients from fluorescence microscopy

Fluorescence microscopy on passivated glass surfaces produce a detailed picture of the two-phase system. As can be seen in Supplementary videos 1 and 2 in the online version at https://doi.org/10.1016/bs.mie.2020.06.007, coacervates nucleate after an incubation period of 5 min and move in and out of the focal plane. For quantitative measurements we use the focal plane near the glass, where coacervates settle and are less mobile, Fig. 4C(i and ii). Due to the different sizes of the coacervates (ranging from 1 to 10 μm radius at the final reaction time), wide-field fluorescence microscopy can be advantageous to remove the variation in droplet midplanes.

Light intensity profiles of both excitation wavelengths were plotted using ImageJ software for the ATP-PLL coacervates. A clear difference in partitioning can be observed between PLL and PyK (Fig. 4C(i)). While TAMRA-labeled PLL completely co-localizes with the observed coacervates from transmission images, PyK labeled with Alexa-647 accumulates at the coacervate interface. The partitioning coefficient (K_p) is determined from the ratio of emission intensity between the inner coacervate region and its surroundings. We use the integrated intensity (I) in a fixed squared area, and correct it for the emission of a blank (same excitation settings, no fluorophore).

$$K_P = \frac{I_{in} - I_{blank}}{I_{out} - I_{blank}} \tag{4}$$

Note that the blank emission can drastically affect K_p. For example, for a droplet with integrated Alexa-647 fluorescence intensity of 100, and an intensity in the surrounding solution of 10, a blank intensity of either 1 or 9 will result in a K_p of 10 or 91. The difference in midplanes also requires that coacervates of different sizes and frame positions, are used for a reliable determination of K_p. Finally, K_p must be measured under equilibrium conditions, and it is therefore crucial to perform the measurement with different droplet incubation times to check for variation.

Using this method, we find a partitioning coefficient of *ca.* 100 for PLL (PLL^{TAMRA}) in ATP-based coacervates. In this case we assume the labeling does not affect partitioning, but that is not necessarily true. Especially in the case of small molecules, such as ATP, attachment of a fluorescent label can

strongly affect its partitioning (Deshpande et al., 2019). Also in the case of enzymes, the degree of labeling of the enzyme, and the hydrophobicity of the label (which can be accessed by its membrane interaction parameter), can completely change properties, including activity, which we did not test for here. One way to find out if labeling affects partitioning is to repeat the labeling with a different fluorophore, for example, with a different charge and/or hydrophobicity, and compare the partitioning coefficients for both labels.

5.4 Concentrations from classical analytical tools

Typical chemical tools for quantification can be used for coacervates if the proper sample preparation steps are taken. NMR and UV/Vis spectroscopy can be performed in the emulsion, but we observe better reproducibility if the phases are separated or the emulsion is dissolved. For partitioning coefficients, macrophase separation is needed; for bulk reaction monitoring, we suggest dissolving the coacervates prior to chromatographic analysis.

Fig. 4D(i) shows the chromatograms of the treated dense and dilute phases of ATP-PLL coacervates. ADP and ATP can be clearly separated with our method, and also PEP and PLL can be detected at 215 nm. After applying the dilution factors, we obtain the partitioning coefficients in Table 1.

An important source of error that remains is the calculation of the coacervate volume. The coacervate volumes are usually small, and relative uncertainties in their quantification can be large. In addition, in our approach we assume that the volume changes upon mixing a high ionic strength solution with a dense coacervate phase are negligible. In our experience, the potential error arising from this assumption is smaller than the typical uncertainties introduced in any of the alternative methods to determine ultrasmall volumes of liquids with unknown densities (Aumiller et al., 2016).

Table 1 Partitioning coefficients obtained using different methodologies.

Component	K_p	Determination method
PLL	98 ± 16	FL-microscopy
PyK enzyme	Interfacial	FL-microscopy
ATP	52 ± 18	HPLC
ADP	18 ± 4	HPLC
PEP	0.8 ± 0.5	HPLC

The accuracy of HPLC also produces a reliable kinetic profile of ATP formation, that can be used to obtain K_M and k_{cat}. Because it requires quenching and dissolution prior to analysis, it is difficult to obtain several time points in the linear range of the kinetic curve, so we recommend fitting the exponential curve to derive the initial velocities. The Michaelis-Menten plot shown in Fig. 4D(ii) reveals that coacervation hardly affected the overall reaction, which can be due to the small number of coacervates. K_M and k_{cat} values can be obtained from the linearization of the plot (and considering an enzyme concentration of 80 nM) and although not remarkably different, they demonstrate that it is possible to perform a typical enzyme-kinetics study with coacervates droplets using our method. Microscopy can be misleading in terms of the ratio between coacervates and solution, but our volume measurements confirm that ATP-PLL coacervates take up no more than 1% of the total mixture volume (10–13 μL for 1000 μL), similar to the volume fraction of PNPase coacervates (1–2 μL for 100 μL). These results also match the micrographs showing that after 10 min, the nucleation of new coacervates seems to stall and only coalescence events are observed. Additional information could be obtained by carrying out the kinetic analysis in the two phases separately, which would be less challenging for coacervates of higher volume fraction, or for fluorogenic enzymatic reactions.

6. Summary and conclusion

To summarize, we have given elaborate protocols and guidelines to study enzymatically controlled coacervation. Dynamic control by enzymes is desirable as coacervates are being used both as promising models to study membraneless organelles, and as synthetic cell models. The transition from passive coacervate droplets toward active and dynamic coacervates brings some additional requirements that have to be taken into account. In this chapter we used a charged-based coacervate system based on ATP-poly-lysine and a length-based coacervate system based on elongation of an oligo-RNA primer by UDP, which phase separates with spermine, as two examples, but the protocols should not be limited to these two systems. The workflow presented here is general and may help in assessing the feasibility of other candidate enzymes as active modulators of coacervation.

Acknowledgment

The authors acknowledge financial support from the Netherlands Organization for Scientific Research (NWO).

Competing interests

The authors declare no competing interests.

References

Aumiller, W. M., Jr., Pir Cakmak, F., Davis, B. W., & Keating, C. D. (2016). RNA-based coacervates as a model for membraneless organelles: Formation, properties, and interfacial liposome assembly. *Langmuir*, *32*(39), 10042–10053. https://doi.org/10.1021/acs.langmuir.6b02499.

Aumiller, W. M., & Keating, C. D. (2015). Phosphorylation-mediated RNA/peptide complex coacervation as a model for intracellular liquid organelles. *Nature Chemistry*, *8*(2), 129–137. https://doi.org/10.1038/nchem.2414.

Banani, S. F., Lee, H. O., Hyman, A. A., & Rosen, M. K. (2017). Biomolecular condensates: Organizers of cellular biochemistry. *Nature Reviews Molecular Cell Biology*, *18*(5), 285–298. https://doi.org/10.1038/nrm.2017.7.

Banerjee, P. R., Milin, A. N., Moosa, M. M., Onuchic, P. L., & Deniz, A. A. (2017). Reentrant phase transition drives dynamic substructure formation in ribonucleoprotein droplets. *Angewandte Chemie International Edition in English*, *56*(38), 11354–11359. https://doi.org/10.1002/anie.201703191.

Beljanski, M. (1996). De novo synthesis of DNA-like molecules by polynucleotide phosphorylase in vitro. *Journal of Molecular Evolution*, *42*(5), 493–499. https://doi.org/10.1007/bf02352279.

Berry, J., Weber, S. C., Vaidya, N., Haataja, M., & Brangwynne, C. P. (2015). RNA transcription modulates phase transition-driven nuclear body assembly. *Proceedings of the National Academy of Sciences of the United States of America*, *112*(38), E5237–E5245. https://doi.org/10.1073/pnas.1509317112.

Brangwynne, C. P., Eckmann, C. R., Courson, D. S., Rybarska, A., Hoege, C., Gharakhani, J., et al. (2009). Germline P granules are liquid droplets that localize by controlled dissolution/condensation. *Science*, *324*(5935), 1729. https://doi.org/10.1126/science.1172046.

Brangwynne, C. P., Tompa, P., & Pappu, R. V. (2015). Polymer physics of intracellular phase transitions. *Nature Physics*, *11*(11), 899–904. https://doi.org/10.1038/nphys3532.

Bungenberg de Jong, H. G., & Kruyt, H. R. (1929). Coacervation (partial miscibility in colloid systems). *Proceedings of the Royal Academy of Sciences at Amsterdam*, *32*, 849–856.

Case, L. B., Zhang, X., Ditlev, J. A., & Rosen, M. K. (2019). Stoichiometry controls activity of phase-separated clusters of actin signaling proteins. *Science*, *363*(6431), 1093–1097. https://doi.org/10.1126/science.aau6313.

Davis, B. W., Aumiller, W. M., Jr., Hashemian, N., An, S., Armaou, A., & Keating, C. D. (2015). Colocalization and sequential enzyme activity in aqueous biphasic systems: Experiments and modeling. *Biophysical Journal*, *109*(10), 2182–2194. https://doi.org/10.1016/j.bpj.2015.09.020.

Deshpande, S., Brandenburg, F., Lau, A., Last, M. G. F., Spoelstra, W. K., Reese, L., et al. (2019). Spatiotemporal control of coacervate formation within liposomes. *Nature Communications*, *10*(1), 1800. https://doi.org/10.1038/s41467-019-09855-x.

Elbaum-Garfinkle, S., Kim, Y., Szczepaniak, K., Chen, C. C., Eckmann, C. R., Myong, S., et al. (2015). The disordered P granule protein LAF-1 drives phase separation into droplets with tunable viscosity and dynamics. *Proceedings of the National Academy of Sciences of the United States of America*, *112*(23), 7189–7194. https://doi.org/10.1073/pnas.1504822112.

Feric, M., Vaidya, N., Harmon, T. S., Mitrea, D. M., Zhu, L., Richardson, T. M., et al. (2016). Coexisting liquid phases underlie nucleolar subcompartments. *Cell*, *165*(7), 1686–1697. https://doi.org/10.1016/j.cell.2016.04.047.

Harmon, T. S., Holehouse, A. S., Rosen, M. K., & Pappu, R. V. (2017). Intrinsically disordered linkers determine the interplay between phase separation and gelation in multivalent proteins. *Elife*, *6*, e30294. https://doi.org/10.7554/eLife.30294.

Kaibara, K., Okazaki, T., Bohidar, H. B., & Dubin, P. L. (2000). pH-induced coacervation in complexes of bovine serum albumin and cationic polyelectrolytes. *Biomacromolecules*, *1*(1), 100–107. https://doi.org/10.1021/bm990006k.

Koga, S., Williams, D. S., Perriman, A. W., & Mann, S. (2011). Peptide-nucleotide microdroplets as a step towards a membrane-free protocell model. *Nature Chemistry*, *3*(9), 720–724. https://doi.org/10.1038/nchem.1110.

Li, P., Banjade, S., Cheng, H. C., Kim, S., Chen, B., Guo, L., et al. (2012). Phase transitions in the assembly of multivalent signalling proteins. *Nature*, *483*(7389), 336–340. https://doi.org/10.1038/nature10879.

Maharana, S., Wang, J., Papadopoulos, D. K., Richter, D., Pozniakovsky, A., Poser, I., et al. (2018). RNA buffers the phase separation behavior of prion-like RNA binding proteins. *Science*, *360*(6391), 918–921. https://doi.org/10.1126/science.aar7366.

Marianelli, A. M., Miller, B. M., & Keating, C. D. (2018). Impact of macromolecular crowding on RNA/spermine complex coacervation and oligonucleotide compartmentalization. *Soft Matter*, *14*(3), 368–378. https://doi.org/10.1039/c7sm02146a.

Mason, A. F., Buddingh, B. C., Williams, D. S., & van Hest, J. C. M. (2017). Hierarchical self-assembly of a copolymer-stabilized coacervate protocell. *Journal of the American Chemical Society*, *139*(48), 17309–17312. https://doi.org/10.1021/jacs.7b10846.

Mitrea, D. M., Chandra, B., Ferrolino, M. C., Gibbs, E. B., Tolbert, M., White, M. R., et al. (2018). Methods for physical characterization of phase-separated bodies and membraneless organelles. *Journal of Molecular Biology*, *430*(23), 4773–4805. https://doi.org/10.1016/j.jmb.2018.07.006.

Mitrea, D. M., Cika, J. A., Guy, C. S., Ban, D., Banerjee, P. R., Stanley, C. B., et al. (2016). Nucleophosmin integrates within the nucleolus via multi-modal interactions with proteins displaying R-rich linear motifs and rRNA. *eLife*, *5*, e13571. https://doi.org/10.7554/eLife.13571.

Mitrea, D. M., Cika, J. A., Stanley, C. B., Nourse, A., Onuchic, P. L., Banerjee, P. R., et al. (2018). Self-interaction of NPM1 modulates multiple mechanisms of liquid-liquid phase separation. *Nature Communications*, *9*(1), 842. https://doi.org/10.1038/s41467-018-03255-3.

Nakashima, K. K., Baaij, J. F., & Spruijt, E. (2018). Reversible generation of coacervate droplets in an enzymatic network. *Soft Matter*, *14*(3), 361–367. https://doi.org/10.1039/c7sm01897e.

Nakashima, K. K., Vibhute, M. A., & Spruijt, E. (2019). Biomolecular chemistry in liquid phase separated compartments. *Frontiers in Molecular Biosciences*, *6*, 21. https://doi.org/10.3389/fmolb.2019.00021.

Nott, T. J., Craggs, T. D., & Baldwin, A. J. (2016). Membraneless organelles can melt nucleic acid duplexes and act as biomolecular filters. *Nature Chemistry*, *8*(6), 569–575. https://doi.org/10.1038/nchem.2519.

Nott, T. J., Petsalaki, E., Farber, P., Jervis, D., Fussner, E., Plochowietz, A., et al. (2015). Phase transition of a disordered nuage protein generates environmentally responsive membraneless organelles. *Molecular Cell*, *57*(5), 936–947. https://doi.org/10.1016/j.molcel.2015.01.013.

Overbeek, J. T. G., & Voorn, M. J. (1957). Phase separation in polyelectrolyte solutions. Theory of complex coacervation. *Journal of Cellular and Comparative Physiology*, *49*(S1), 7–26. https://doi.org/10.1002/jcp.1030490404.

Perry, S. L., & Sing, C. I. (2015). PRISM-based theory of complex coacervation: Excluded volume versus chain correlation. *Macromolecules*, *48*, 5040–5053. https://pubs.acs.org/doi/abs/10.1021/acs.macromol.5b01027#.

Qamar, S., Wang, G., Randle, S. J., Ruggeri, F. S., Varela, J. A., Lin, J. Q., et al. (2018). FUS phase separation is modulated by a molecular chaperone and methylation of arginine cation-pi interactions. *Cell*, *173*(3), 720–734 e715. https://doi.org/10.1016/j.cell.2018.03.056.

Quinn, M. K., Gnan, N., James, S., Ninarello, A., Sciortino, F., Zaccarelli, E., et al. (2015). How fluorescent labelling alters the solution behaviour of proteins. *Physical Chemistry Chemical Physics*, *17*(46), 31177–31187. https://doi.org/10.1039/c5cp04463d.

Rai, A. K., Chen, J. X., Selbach, M., & Pelkmans, L. (2018). Kinase-controlled phase transition of membraneless organelles in mitosis. *Nature*, *559*(7713), 211–216. https://doi.org/10.1038/s41586-018-0279-8.

Saito, M., Hess, D., Eglinger, J., Fritsch, A. W., Kreysing, M., Weinert, B. T., et al. (2019). Acetylation of intrinsically disordered regions regulates phase separation. *Nature Chemical Biology*, *15*(1), 51–61. https://doi.org/10.1038/s41589-018-0180-7.

Schuster, B. S., Reed, E. H., Parthasarathy, R., Jahnke, C. N., Caldwell, R. M., Bermudez, J. G., et al. (2018). Controllable protein phase separation and modular recruitment to form responsive membraneless organelles. *Nature Communications*, *9*(1), 2985. https://doi.org/10.1038/s41467-018-05403-1.

Semenov, S. N., Wong, A. S., van der Made, R. M., Postma, S. G., Groen, J., van Roekel, H. W., et al. (2015). Rational design of functional and tunable oscillating enzymatic networks. *Nature Chemistry*, 7(2), 160–165. https://doi.org/10.1038/nchem.2142.

Shin, Y., & Brangwynne, C. P. (2017). Liquid phase condensation in cell physiology and disease. *Science*, *357*(6357), eaaf4382. https://doi.org/10.1126/science.aaf4382.

Sokolova, E., Spruijt, E., Hansen, M. M., Dubuc, E., Groen, J., Chokkalingam, V., et al. (2013). Enhanced transcription rates in membrane-free protocells formed by coacervation of cell lysate. *Proceedings of the National Academy of Sciences of the United States of America*, *110*(29), 11692–11697. https://doi.org/10.1073/pnas.1222321110.

Spoelstra, W. K., van der Sluis, E. O., Dogterom, M., & Reese, L. (2020). Non-spherical coacervate shapes in an enzyme driven active system. *Langmuir*, *36*, 1956–1964. https://doi.org/10.1021/acs.langmuir.9b02719.

Spruijt, E., Westphal, A. H., Borst, J. W., Cohen Stuart, M. A., & van der Gucht, J. (2010). Binodal compositions of polyelectrolyte complexes. *Macromolecules*, *43*(15), 6476–6484. https://doi.org/10.1021/ma101031t.

Su, X., Ditlev, J. A., Hui, E., Xing, W., Banjade, S., Okrut, J., et al. (2016). Phase separation of signaling molecules promotes T cell receptor signal transduction. *Science*, *352*(6285), 595–599. https://doi.org/10.1126/science.aad9964.

Te Brinke, E., Groen, J., Herrmann, A., Heus, H. A., Rivas, G., Spruijt, E., et al. (2018). Dissipative adaptation in driven self-assembly leading to self-dividing fibrils. *Nature Nanotechnology*, *13*(9), 849–855. https://doi.org/10.1038/s41565-018-0192-1.

Wang, J. T., Smith, J., Chen, B. C., Schmidt, H., Rasoloson, D., Paix, A., et al. (2014). Regulation of RNA granule dynamics by phosphorylation of serine-rich, intrinsically disordered proteins in C. elegans. *Elife, 3*, e04591. https://doi.org/10.7554/eLife.04591.

Wei, M. T., Elbaum-Garfinkle, S., Holehouse, A. S., Chen, C. C., Feric, M., Arnold, C. B., et al. (2017). Phase behaviour of disordered proteins underlying low density and high permeability of liquid organelles. *Nature Chemistry*, *9*(11), 1118–1125. https://doi.org/10.1038/nchem.2803.

Yewdall, N. A., Buddingh, B. C., Altenburg, W. J., Timmermans, S., Vervoort, D. F. M., Abdelmohsen, L., et al. (2019). Physicochemical characterization of polymer-stabilized coacervate protocells. *Chembiochem*, *20*(20), 2643–2652. https://doi.org/10.1002/cbic.201900195.

Zwicker, D., Seyboldt, R., Weber, C. A., Hyman, A. A., & Jülicher, F. (2016). Growth and division of active droplets provides a model for protocells. *Nature Physics*, *13*(4), 408–413. https://doi.org/10.1038/nphys3984.